

**DISCOVERY OF MARTENSITIC TRANSFORMATION
TEMPERATURE WITH A CRITICAL e/a RATIO IN Ni-Mn-Ga
HEUSLER ALLOYS**

A PROJECT SUBMITTED TO GOA UNIVERSITY FOR THE AWARD OF THE
DEGREE OF

MASTER OF SCIENCE

IN

PHYSICS

BY

VISHWAS VENKATESH PRABHU

AND

DISHA SANTOSH SINAI SANGAONKAR

PROJECT GUIDE

DR. K. R. PRIOLKAR

GOA UNIVERSITY

TALEIGAO GOA

(2022)

DECLARATION

We hereby declare that the project work entitled “Discovery of Martensitic Transformation Temperature with a Critical c/a Ratio in Ni-Mn-Ga Heusler Alloys”, as a final year M.Sc. project, submitted to the Department of Physics, School of Physical and Applied Science, Goa University, is an authentic record of our bonified work carried out under the guidance of Dr. Kaustubh R. S. Priolkar. I further declare that the work reported in this project has not been submitted, either in part or full, for the award of any other degree or diploma in this university or any other university.

Date: May 2022

Vishwas V. Prabhu

Place: Goa University

Disha S. S. Sangaonkar

School of Physical and Applied Science

Department of Physics

ACKNOWLEDGEMENT

It is indeed our privilege to thank all those involved directly or indirectly and contributed to the success of our work.

First, we would like to express our special appreciation and deep sense of gratitude to our respected guide, Dr. Kaustubh R. S. Priolkar, Professor, Department of Physics and Dean of School of Physical and Applied Science, Goa University, who has supported and guided us throughout our project with his knowledge. He encouraged us to get to the bottom of every problem and helped us to understand it fully by providing all the necessities, without which this project would not have been complete.

We would like to thank Mr. Nafea Bhlos, Research Scholar, for his continuous help, guidance and support in all the experimental parts of our project.

We like to thank Dr. Sudhir Cherukulappurath, Assistant Professor, Head of Department of Physics, Goa University, for making all the necessary facilities available for the project.

We are thankful to Dr. Venkatesha R. Hathwar, Assistant Professor, Department of Physics, for his help and guidance with experimental XRD characterisation.

A note of thanks to the Lab Technician, Department of Electronics, Mr. Vishant Malik, for his help and cooperation while doing EDAX experimental characterisation.

I would also like to thank all the teaching and non-teaching staff of the Department of Physics for their cooperation and constant help.

Special thanks to my parents and M.Sc. friends, for their encouragement, constant support and cooperation, emotionally and financially during our project.

CERTIFICATE

This is to certify that the project entitled

**DISCOVERY OF MARTENSITIC TRANSFORMATION
TEMPERATURE WITH A CRITICAL e/a RATIO IN Ni-Mn-Ga
HEUSLER ALLOYS**

being submitted by

Vishwas Venkatesh Prabhu

And

Disha Santosh Sinai Sangaonkar

in the partial fulfilment of the degree of

MASTER OF SCIENCE IN PHYSICS

Goa University

is a record of their own work carried out in the department

Project Supervisor

[Dr. Kaustubh R. Priolkar]

Programme Director

[Dr. Sudhir Cherukulappurath,]

CONTENTS

DECLARATION	I
ACKNOWLEDGEMENT	II
CERTIFICATE.....	III
CHAPTER 1	1
INTRODUCTION	1
1.1 HISTORICAL BACKGROUND.....	1
1.2 SHAPE MEMORY ALLOYS	1
1.3 PHENOMENA OF PHASE TRANSFORMATION	2
1.4 MAGNETIC SHAPE MEMORY ALLOYS	4
1.5 FACTORS AFFECTING MARTENSITIC TRANSFORMATION	6
1.6 ELECTRON PER ATOM RATIO	7
1.7 AIM OF THE PROJECT	8
REFERENCES	10
CHAPTER 2	12
EXPERIMENTAL TECHNIQUES	12
2.1 SAMPLE PREPARATION TECHNIQUE	12
2.1.1 Sample Preparation Calculations	14
2.2 ENERGY DISPERSIVE ANALYSIS OF X-RAY (EDAX).....	15
2.3 X-RAY DIFFRACTION (XRD)	18
2.3.1 Production of X-ray	19
2.4 FOUR PROBE RESISTIVITY	21
REFERENCES	23
CHAPTER 3	25
RESULT AND DISCUSSION	25
3.1 EDAX	25
3.2 XRD DATA	27
3.3 RESISTIVITY	30
CHAPTER 4.....	33
4.1 CONCLUSION.....	33

+

CHAPTER 1

INTRODUCTION

1.1 HISTORICAL BACKGROUND

Martensite, named after the German metallurgist Adolf Martens (1850-1914) studied samples of different steels under a microscope. With his discovery of martensite in steels in the 1890s he put forward, the first step towards the discovery of shape memory alloys and was perhaps the most widely studied metallurgical phenomenon during the early 1900s. The first recorded observation of shape memory transformation was by Chang and Read in 1932.^[1] They noted the reversibility of the transformation in AuCd by metallographic observations and resistivity changes. In 1938, the transformation was seen in brass (CuZn). The concept of thermoelastic martensitic transformation, which explained the reversible transformation of martensite, was introduced in 1949 by Kurd-jumov and Khandros, based on experimental observations on CuZn and CuAl alloys. In 1951 the shape memory effect (SME) was observed in a bent bar of AuCd.^[2]

1.2 SHAPE MEMORY ALLOYS

Shape Memory Alloys (SMAs), are a class of metallic materials that 'remember' their shape and have the ability to pre-deform to it when subjected to the appropriate thermal procedure. Generally, at relatively low temperature, these materials can be plastically deformed, and upon exposure to some higher temperature will return to their shape prior to the deformation. Some materials exhibit shape memory only upon heating are referred as one-way shape memory and some materials undergo a change in shape upon re-cooling referred as two-way shape memory. The key attributes of SMAs are pseudo elasticity and shape memory effect. These amusing properties are due to a temperature-dependent phase transformation, from a highly symmetric to a low-symmetry crystallographic structure. The martensitic

transformation exhibits well-defined characteristics that distinguish it from among other solid-state transformations:

- It is associated with an inelastic deformation of the crystal lattice with no diffusive process involved, making martensitic phase transformation almost instantaneous. The phase transformation results from a cooperative and collective motion of atoms on distances smaller than the lattice parameters.
- Since it is a first order transition parent and product phases coexist during the phase transformation, but separated by an invariant plane.
- Transformation of a unit cell element produces a volumetric and a shear strain along well-defined plane. The shear strain can be many times larger than the elastic distortion of the unit cell. This transformation is crystallographically reversible.
- Since the crystal lattice of the martensitic phase has lower symmetry than that of the parent austenitic phase, several variants of martensite can be formed from the same parent phase crystal.
- Temperature, stress and pressure have a large influence on the martensitic transformation.^[1]

1.3 PHENOMENA OF PHASE TRANSFORMATION

Austenite and Martensite are the two phases which occur in shape memory alloys. In the austenite, the high temperature phase, the lattice structure is cubic Fig.1.3.1(a) (Ni_2MnGa). Martensite, the lower temperature phase, is relatively soft and easily deformable. The molecular structure in this phase is twinned, shown in Fig 1.3.1(b). The undeformed Martensite phase is of same size and shape as Austenite phase on a macroscopic scale, so that no change in size or shape is there in shape memory alloys until the Martensite is deformed. If mechanical load is applied to twinned martensite (at low temperature) it is possible to detwin the martensite. Upon releasing of the load, the material remains deformed, until

heating of the material to a temperature above A_f which will result in reverse phase transformation (martensite to austenite) and will lead to complete shape recovery, as shown in Figure 1.3.2. The above-described process results in manifestation of the Shape Memory Effect (SME), and the solid-state phase change that takes place through the atomic rearrangement is known as Martensitic Transformation. It is also possible to induce a martensitic transformation which would lead directly to detwinned martensite, thereby applying load in the austenite phase and the material is cooled, giving rise to the phase transformation which will result in detwinned martensite. Thus, very large strains will be observed. Reheating the material will result in complete shape recovery. Higher values of the applied load will lead to higher values of the transformation temperatures. The above-described loading path is shown in Figure 1.3.3. The temperatures at which austenite starts to convert into martensite is known as M_s - martensitic start and the temperature when it fully converts is known as M_f - martensitic finish. The reverse process in which a martensite begins to transform to austenite and the temperature it fully converts into austenite are known as A_s - austenitic start and A_f - austenitic finish respectively.^[3]

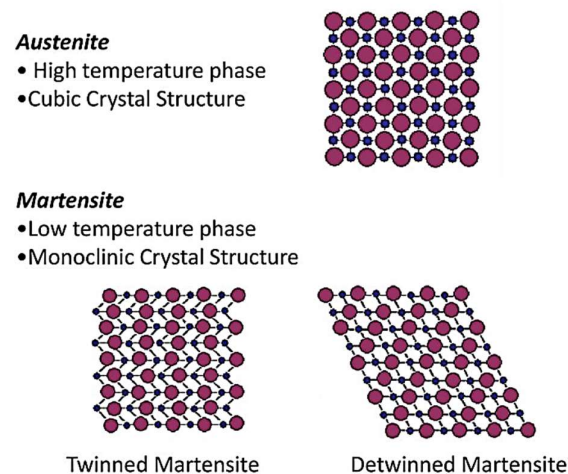


Figure 1.3.1: Structural phases of a shape memory alloy.³

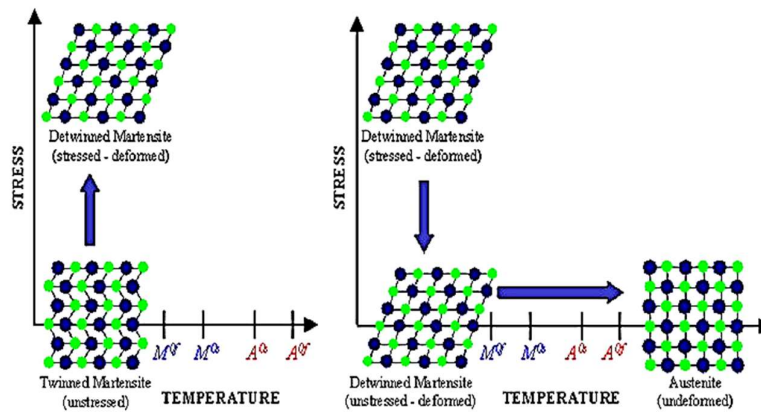


Figure 1.3.2: Shape Memory Effect of an SMA showing (left hand side figure) detwinning of the material with an applied load and (right hand side figure) the unloading and subsequent heating to austenite under no load.^[3]

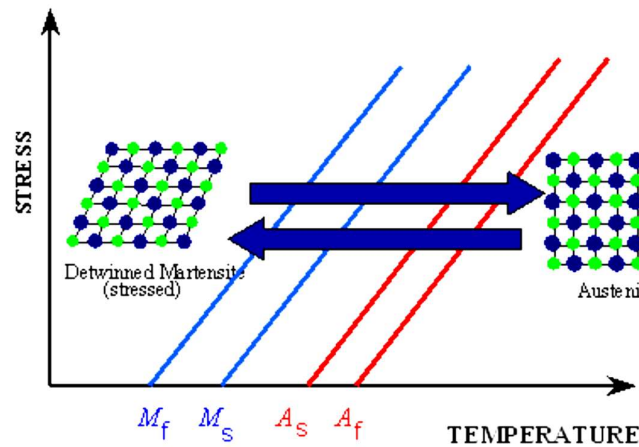


Figure 1.3.3: Temperature-induced phase transformation with applied load.^[3]

1.4 MAGNETIC SHAPE MEMORY ALLOYS

In the case when shape memory alloys are magnetic, they may exhibit magnetic shape memory effect (MSM). Such an effect was first discovered in Heusler alloys. Heusler alloys was first discovered by a German chemist Fredrich Heusler in 1903. They are the magnetic intermetallic with fcc crystal structure having composition of XYZ and X_2YZ known as half Heusler in the $C1_b$ structure and full Heusler in $L2_1$ structure, which consist of four fcc sub lattices respectively. $C1_b$ structure is formed by removing one of the X sites. Ferromagnetic shape memory alloys (FMSA's) offer an ability to cause quick transition by means of an

applied magnetic field rather than the slow process of shape change by temperature, thereby combining high strains with fast reaction times.^[4] X and Y are 3d elements and Z is a group IIIA–VA element. These alloys show magnetism which is due to the X and/or Y elements.^{[5],[6]}

One of the most common types of FSMA alloy studied is Ni₂MnGa for its potential in commercial use. In its stoichiometric composition, ferromagnetic Ni₂MnGa undergoes a martensitic transformation from a L2₁ cubic structure to an orthorhombic state at T_M ~220 K.^[7] Ni-Mn based alloys are very sensitive to the elemental composition of the samples thereby affecting strongly to the temperatures of phase transformations and the formation of superstructures in the austenitic and martensitic states.^[8] In the austenite state, Heusler alloys have an L2₁ structure (space group *Fm.3m*) which consists of four interpenetrating fcc sublattices, as shown in figure 1.4.1(a).^[9] For the stoichiometric composition, Ni atoms occupy the 8c positions (in Wyckoff notation), while Mn and Z atoms occupy 4a and 4b positions, respectively.^[10] When the temperature is decreased, they can undergo a martensitic transformation and acquire a number of structures. In particular, Ni–Mn–Z Heusler alloys (Z: Ga), at low Z concentrations they transform to the L1₀ tetragonal structure, the relationship between the L2₁ and the tetragonal structures is given in figure 1.4.1(a) and the tetragonal structure is also shown separately in figure 1.4.1(b).^[9]

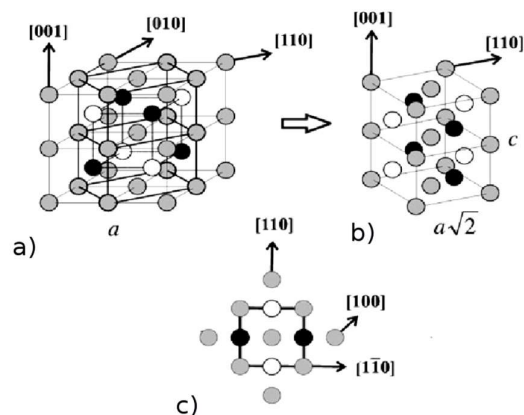


Figure 1.4.1: Austenite and martensite structures of Heusler alloys shown for the case of Ni₂MnGa. Light grey: Ni, white: Mn, black: Ga. (a) The L2₁ Heusler structure showing also the relationship with the tetragonal unit cell, which is also shown in part (b). (c) The tetragonal unit cell viewed from the top.^[10]

Figure 1.4.1 can depict Ni₂MnGa since, across the transition almost no volume change occurs.^{[11],[12]} Similar structures are seen in other Ni-Mn-Z Heusler alloys undergoing martensitic transformations, but it takes place at off stoichiometric compositions, depending on the Z species and volume changes across the martensitic transition.^{[13],[14]} This introduces complexities in depicting the crystallographic relationships between the austenitic and martensitic states in alloys with Z species other than Ga, which is principally straightforward for Ni₂MnGa.^[15] The martensitic phase stability of Ni-Mn-Z alloys is decided by its composition.

1.5 FACTORS AFFECTING MARTENSITIC TRANSFORMATION

The mechanical properties of single crystal Ni-Mn-Ga alloy specimens vary significantly due to strong dependence on crystal structure and material composition affecting the martensite start M_s , martensite finish M_f , austenite start A_s , and austenite finish A_f temperatures respectively. Thereby, affecting Martensitic transformation temperature. Wu et al,^[20] studied the effect of transformation temperatures for Ni-Mn-Ga alloys. Ni and Ga have a major impact on martensitic transformation temperatures. Increasing the Ni content at the expense of Ga content increases the T_M temperature. On the other hand, reducing the Ni and increasing the Ga content tends to decrease the M_s , M_f , A_s and A_f temperatures.^[20] G.D. Liu studied that for some alloys, reducing the Ni and Increasing the Mn, decreases the martensitic transformation, hence decreasing the e/a ratio.^[21]

1.6 ELECTRON PER ATOM RATIO

The martensitic structures and transformation temperatures have been determined as the functions of electron per atom concentration (e/a). The (e/a) ratio of the average electrons per atom in the unit cell and it depends on the valence electron available from each atom present in the unit cell.^{[16],[17],[18]}

$$\frac{e}{a} = \frac{10 \times (\text{Ni at}\%) + 7 \times (\text{Mn at}\%) + X \times (\text{Z at}\%)}{(\text{Ni at}\% + \text{Mn at}\% + \text{Z at}\%)}$$

Where, Z = (In, Sn, Sb and Ga).

X = Valence electron of Z.

For e.g., Ni₂MnGa

$$\frac{e}{a} = \frac{10 \times (2) + 7 \times (1) + 3 \times (1)}{(4)} = 7.5$$

In this case valence electrons for Ni, Mn and Ga are 10, 7 and 3 respectively, multiplied by the concentration of each element, and further divided by total elemental composition.

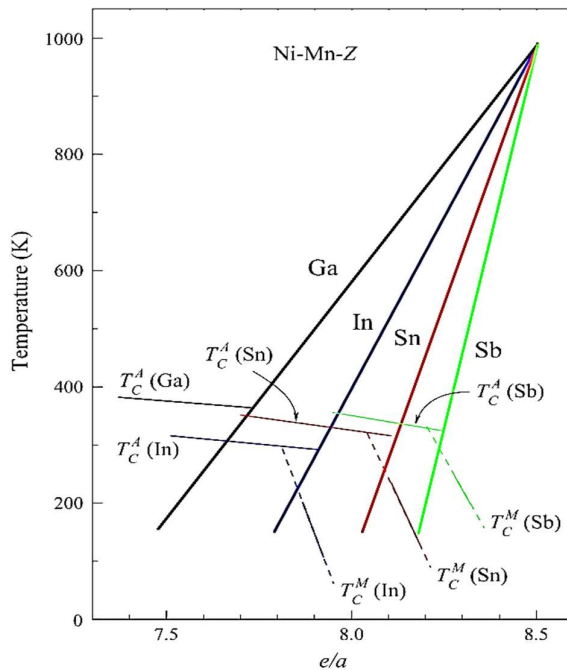


Figure 5.1: The e/a dependence of Martensitic Transition temperature M_S for Ni-Mn-Z alloys for Z = Ga, In, Sn and Sb.^[16]

Figure 5.1, shows e/a dependence of martensitic transition temperature. The above graph clearly shows that, for Sb, Sn, In and Ga the slope of the graph decreases as e/a is decreased, thereby decreasing the martensitic transition temperature. It appears that there is a critical e/a concentration for In (7.85), Sn (8), Sb (8.2) for the appearance of martensitic transition temperature. Below this e/a martensitic transition disappears fully. But in the case of Ga they found that it shows martensitic transformation till 7.5 e/a and also below 7.5. In the above graph they haven't checked below 7.5 e/a whether there is any critical e/a value, for which martensitic transformation disappears.^[16]

1.7 AIM OF THE PROJECT

Literature survey was conducted on Ni-Mn-Z alloys. Figure 1.6.1 shows the structural phase transition temperatures of Ni-Mn-Z Heusler alloys with Z as Ga, In, Sn and Sb plotted as a function of the valence electron concentration per atom (e/a).^{[10],[19]}

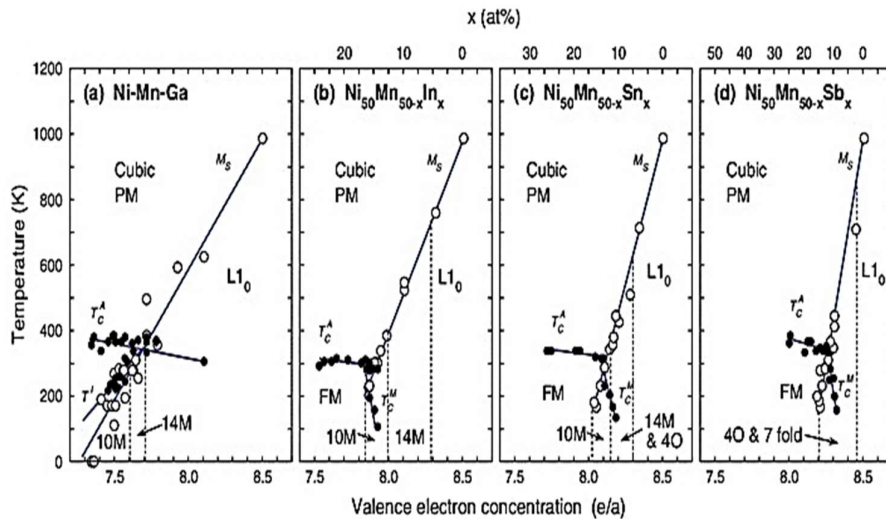


Figure 1.6.1: The magnetic and structural phase diagram of Ni-Mn-Z Heusler alloys with Z as (a) Ga, (b) In, (c) Sn and (d) Sb. The triangles and the circles correspond to the magnetic and martensitic transition temperatures respectively. The regions corresponding to the different structures are separated by discontinuous lines. Small solid circles in (c) correspond to the pre-martensitic transition temperature.^{[10],[19]}

As seen from the graph we observe that the martensitic transition temperature increases linearly with e/a ratio. By changing the stoichiometric composition of the alloy, e/a ratio can be changed. In the case of Ni_2MnGa which is martensitic, below RT at 220 K, we can vary the e/a ratio by changing the concentration of Ga with Mn, Ni with Ga and Ni with Mn respectively.

The purpose of our project is to prepare six samples as Mn: Ga, Ni: Mn, Ni: Ga by varying e/a ratio below 7.5 and to find the critical e/a ratio at which martensitic transition occurs.

REFERENCES

- [1] Chang, L. C., and T. A. Read. "Behavior of the elastic properties of AuCd." *Trans Met Soc AIME* 191 (1951): 47.
- [2] Kurdjumov, G. V. "The nature of martensitic transformations." *JOM* 11.7 (1959): 449-453.
- [3] Texas, A. M. "Smart Lab,,Introduction to Shape Memory Alloys “.” (2006).
- [4] Ullakko, Kari, et al. "Large magnetic-field-induced strains in Ni₂MnGa single crystals." *Applied Physics Letters* 69.13 (1996): 1966-1968.
- [5] Caroli, B., and A. Blandin. "Champs hyperfins dans les alliages d'Heusler." *Journal of Physics and Chemistry of Solids* 27.3 (1966): 503-508.
- [6] Price, D. C. "Indirect magnetic coupling between local moments in metals." *Journal of Physics F: Metal Physics* 8.5 (1978): 933.
- [7] Zheludev, A., et al. "Phonon anomaly, central peak, and microstructures in Ni₂MnGa." *Physical Review B* 51.17 (1995): 11310.
- [8] Rama Rao, N. V., V. Chandrasekaran, and K. G. Suresh. "Effect of Ni/Mn ratio on phase transformation and magnetic properties in Ni–Mn–In alloys." *Journal of Applied Physics* 108.4 (2010): 043913.
- [9] Planes, Antoni, Lluís Mañosa, and Mehmet Acet. "Magnetocaloric effect and its relation to shape-memory properties in ferromagnetic Heusler alloys." *Journal of Physics: Condensed Matter* 21.23 (2009): 233201.
- [10] Webster, P. J., et al. "Magnetic order and phase transformation in Ni₂MnGa." *Philosophical Magazine B* 49.3 (1984): 295-310.
- [11] Ullakko, Kari, et al. "Large magnetic-field-induced strains in Ni₂MnGa single crystals." *Applied Physics Letters* 69.13 (1996): 1966-1968.
- [12] Ranjan, Rajeev, et al. "Powder x-ray diffraction study of the thermoelastic martensitic transition in Ni₂Mn_{1.05}Ga_{0.95}." *Physical Review B* 74.22 (2006): 224443.
- [13] Krenke, Thorsten, et al. "Inverse magnetocaloric effect in ferromagnetic Ni–Mn–Sn alloys." *Nature materials* 4.6 (2005): 450-454.

- [14] Aksoy, Seda, et al. "Magnetization easy axis in martensitic Heusler alloys estimated by strain measurements under magnetic field." *Applied Physics Letters* 91.25 (2007): 251915.
- [15] Planes, Antoni, LluísMañosa, and Mehmet Acet. "Magnetocaloric effect and its relation to shape-memory properties in ferromagnetic Heusler alloys." *Journal of Physics: Condensed Matter* 21.23 (2009): 233201.
- [16] Pons, J., et al. "Crystal structure of martensitic phases in Ni–Mn–Ga shape memory alloys." *ActaMaterialia* 48.12 (2000): 3027-3038.
- [17]Chernenko, V. A. "Compositional instability of β -phase in Ni-Mn-Ga alloys." *ScriptaMaterialia* 40.5 (1999): 523-527.
- [18]Jin, X., et al. "Empirical mapping of Ni–Mn–Ga properties with composition and valence electron concentration." *Journal of Applied Physics* 91.10 (2002): 8222-8224.
- [19]Sutou, Y., et al. "Magnetic and martensitic transformations of NiMnX (X= In, Sn, Sb) ferromagnetic shape memory alloys." *Applied Physics Letters* 85.19 (2004): 4358-4360.
- [20] Wu, S. K., and S. T. Yang. "Effect of composition on transformation temperatures of Ni–Mn–Ga shape memory alloys." *Materials Letters* 57.26-27 (2003): 4291-4296.
- [21] Liu, G. D., et al. "Martensitic transformation and shape memory effect in a ferromagnetic shape memory alloy: Mn₂NiGa." *Applied Physics Letters* 87.26 (2005): 262504.

CHAPTER 2

EXPERIMENTAL TECHNIQUES

2.1 SAMPLE PREPARATION TECHNIQUE

The arc-melting technique is a primary method used for melting metals in order to form alloy. Approximately 2 grams of polycrystalline off stoichiometric Heusler alloy of $\text{Ni}_2\text{Mn}_{1-x}\text{Ga}_{1+x}$, $\text{Ni}_{2-x}\text{Mn}_{1+x}\text{Ga}$, $\text{Ni}_{2-x}\text{MnGa}_{1+x}$ were prepared by arc-melting high purity (99.99%) constituent elements.^[1]

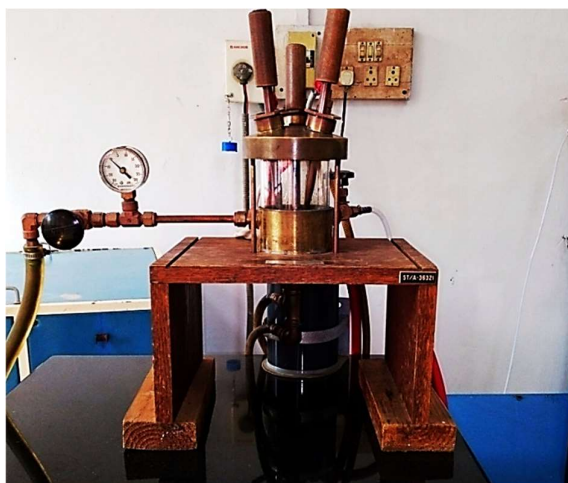


Fig.2.1.1: Arc Melting Unit

An arc-melting furnace (Fig 2.1.1) consists of 3 main parts: power source (TIG-600amp), chiller and vacuum unit. The vacuum unit with rotary and diffusion pump attains a vacuum of 10^{-3} bar. The cold circulation water from the chiller cools both the copper hearth and the tungsten electrode.^[2]

The appropriate amount of constituent elements was kept in the Cu crucible inside a closed chamber. The air inside the chamber is evacuated out by a rotary pump followed by flushing of argon gas through the chamber. The process is repeated 3-4 times in order to ensure the O_2 free environment.^[1]

A tungsten inert gas welding unit is used to provide power to an electrode. Due to high voltage difference maintained between the electrode and the copper hearth, an arc can be generated when the electrode strikes the hearth. The electric arc generates a large amount of heat concentrated near the sample, which melts the metal together into an ingot in the presence of argon gas. When the metal melts it resembles button shape due to surface tension effect. The button shape alloy was again re-melted number of times in order to get homogeneous composition.^[2]

The prepared sample is then polished and cut into two halves using a diamond cutter. One half, is crushed into powder using mortar pestle for X-ray diffraction and other half pieces of alloys are cut afterwards in an appropriate size for various characterisation measurements. Further the crushed powder is wrapped in tantalum foil. Both, the foil wrapped samples and other half were encapsulated in vacuum sealed quartz ampoule. The next step is to anneal the prepared sample at 750⁰C for 48 hours, followed by rapid quenching in ice-water.^[3]



Fig 2.1.2: Quartz tubes containing samples

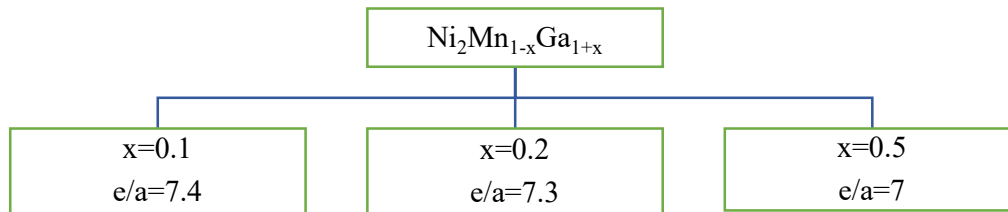
2.1.1 Sample Preparation Calculations

The valence electron concentration per atom (e/a)

$$\frac{e}{a} = \frac{10 \times (\text{Ni at}\%) + 7 \times (\text{Mn at}\%) + 3 \times (\text{Ga at}\%)}{(\text{Ni at}\% + \text{Mn at}\% + \text{Ga at}\%)}$$

Here, the value of 10 is applied for nickel, in which the outer electron shells are occupied as $3d^8 4s^2$, while for manganese the value becomes 7 from $3d^5 4s^2$ and for gallium 3 from $4s^2 4p^1$.

1-



2- $\text{Ni}_{1.73}\text{Mn}_{1.27}\text{Ga}_1$

$$\frac{e}{a} = \frac{10 \times 1.73 + 7 \times 1.27 + 3 \times 1}{4} = 7.297$$

3- $\text{Ni}_{1.88}\text{Mn}_1\text{Ga}_{1.12}$

$$\frac{e}{a} = \frac{10 \times 1.88 + 7 \times 1 + 3 \times 1.12}{4} = 7.29$$

4- $\text{Ni}_2\text{Mn}_{0.85}\text{Ga}_{1.15}$

$$\frac{e}{a} = \frac{10 \times 2 + 7 \times 0.85 + 3 \times 1.15}{4} = 7.35$$

2.2 ENERGY DISPERSIVE ANALYSIS OF X-RAY (EDAX)

EDAX is an investigation method employed in elemental analysis or chemical characterisation and also to identify the elemental composition of a sample. It depends on the interactions between the source of X-ray excitation and sample. Each element exhibits unique atomic structure allowing unique set of peaks on its electromagnetic emission spectrum and due to this fundamental principle, it shows characterisation capabilities.^[4]

To produce characteristic x-ray from a specimen, it is bombarded by either highly energetic beam of charge carriers (electrons or protons) or x-rays. At rest an atom within the sample contains ground state (unexcited) electrons in a discrete energy levels or electron shell bound to the nucleus. An electron from an inner shell may be excited by an incident beam there by removing it from its shell and generating a hole where electron was present before excitation. This hole can be occupied by a higher energy electron from an outer shell. The difference in energies of the higher and lower energy shell is emitted as an x-ray.^[5]

Quantitative measurement of the energy and number of these x-rays emitted can be done with energy dispersive spectrometer. Since the energy of these x-rays is characteristic feature of energy difference between two shells and atomic structure of discharging element. EDAX can be employed to identify the elemental composition of a sample.

The output of an EDX analysis is an EDX spectra, that shows the plot of how frequently an X-ray is received for each energy level. Each of these peaks are unique to an atom, and therefore corresponds to a single element. The higher peak in a spectrum represents the more concentrated element is in the specimen. An EDX spectrum plot not only identifies the element corresponding to each of its peaks, but the type of X-ray to which it corresponds as well.^[5]

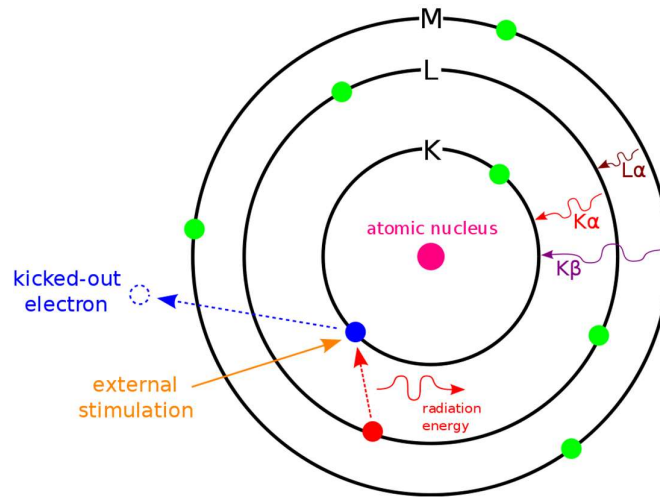


Fig 2.2.1: principle of characteristic X-rays generation [8]

Primary components of EDAX instruments are

- Electron beam source:

EDAX is inbuilt within the Scanning Electron Microscope, therefore the same electron gun is used as an incident electron source and along with this aperture, it is equipped with beam lenses to focus the beam of electrons. The electron beam energy has to be wisely selected to overcome the compromise between the resolution requirements and the production efficiency of x-rays, which are detected by two crystal spectrometers.

- X-ray detector:

EDAX detector measures abundance of emitted X-rays versus X-rays energies. A detector is a solid-state device which is based on lithium drifted silicon. When the X-rays produced from the sample hits the detector, which creates a charge pulse in the detector. This charge pulse is directly proportional to the energy of the incidental X-rays.

- Pulse Processor:

The charge pulse from the detector is converted into voltage pulse by using charge sensitive pre-amplifier.

- Analyser:

Multi-channel analysers are used to sort pulses by voltage in the signals received by the analyser. By measuring the voltage of the charged pulses, the energy of the X-rays can be obtained. The obtained energy is then sent for display and data processing.^[5]

2.3 X-RAY DIFFRACTION (XRD)

X-ray diffraction is a rapid analytical technique for the study of crystal structure of material. X-ray diffraction is based on constructive interference of monochromatic X-rays and a crystalline sample. These X-rays are generated by a cathode ray tube, filtered to produce monochromatic radiation, collimated to concentrate, and directed toward the sample. Diffraction occurs when the Bragg condition which states that, the X-rays reflected from different parallel planes of a crystal interfere constructively when the path difference is integral multiple of the X-ray wavelength, is satisfied(Fig 2.2.2)

i.e., Bragg's Equation, $2d\sin\theta = n\lambda$,

Where n is an integer, λ is the x ray wavelength, d is the inter planar spacing, θ is the diffraction angle. This law relates the wavelength of electromagnetic radiation to the diffraction angle and the lattice spacing in a crystalline sample. These diffracted X-rays are then detected, processed and counted.^[6]

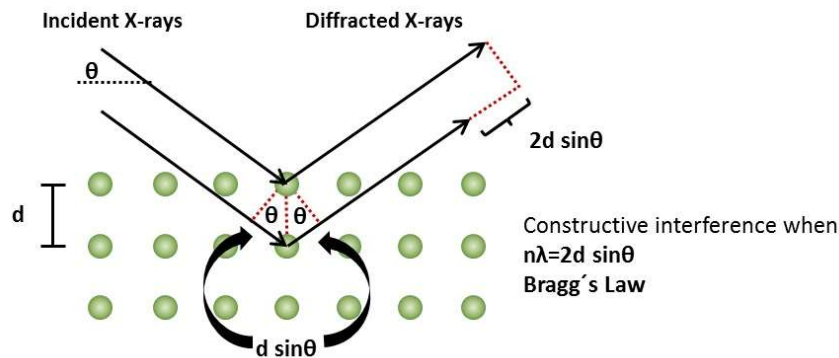


Fig 2.3.1 Braggs Law^[9]

An X-ray diffraction can be carried out on the polycrystalline (powder) samples or single crystals. in powder method, material to be studied is reduced to very fine powder and placed in a beam of monochromatic x-ray. Each particle of the powder is tiny crystal oriented in random direction with respect to incident beam. Due to random direction of the particles

Braggs reflection condition is satisfied for all the lattice planes. Thus, by scanning the sample through a range of 2θ angles, all possible diffraction directions of the lattice should be attained.^[6]

2.3.1 Production of X-ray

X-ray diffractometer consist of three basic elements: x-ray tube, a sample holder and an X-ray detector. A high voltage between cathode and Anode is maintained in vacuum. Cathode is filament of tungsten and anode is water cooled block of copper containing desired target metal like Al, Mn, Mg etc. By heating filament electrons are generated and accelerated towards a target by applying a voltage, and bombarding the target material with electrons. On striking the target electrons transfer their kinetic energy to its metallic surface and knock out the core electrons generating hole. When higher orbit electrons jump into the hole generated in core orbits characteristic x-ray spectra are produced.

These spectra consist of several components, mainly, K_{α} and K_{β} . K_{α} consists in parts, of $K_{\alpha 1}$ and $K_{\alpha 2}$. $K_{\alpha 1}$ has a slightly shorter wavelength and twice the intensity of $K_{\alpha 2}$. The target material (Cu, Fe, Mo, Cr) are characterised by specific wavelengths. Monochromatic X-rays needed for diffraction are produced by using crystal monochromators or filtering by foils. Wavelength of $K_{\alpha 1}$ and $K_{\alpha 2}$ is sufficiently close, due to which weighted average of the two is used. Copper is the most common target material for single-crystal diffraction, with Cu K_{α} radiation $D = 1.5418 \text{ \AA}$.

These X-rays are collimated and directed onto the sample. As the sample and detector are rotated, the intensity of the reflected X-rays is recorded. When the geometry of the incident X-rays impinging the sample satisfies Bragg's law, constructive interference occurs and a peak in intensity appears. A detector records and processes this X-ray signal and converts the signal to a count rate, which is then output to a device such as a printer or computer monitor. The geometry of an X-ray diffractometer is such that the sample rotates in the path of the

collimated X-ray beam at an angle θ while the X-ray detector is mounted on an arm to collect the diffracted X-rays and rotates at an angle of 2θ (Fig 2.3.2). The instrument used to maintain the angle and rotate the sample is termed a goniometer. For typical powder patterns, data are collected at 2θ from 10° to 80° , angles that are preset in the X-ray scan. With specialized techniques, X-ray diffraction (XRD) can be used to determine crystal structures by using Rietveld refinement.^[6]

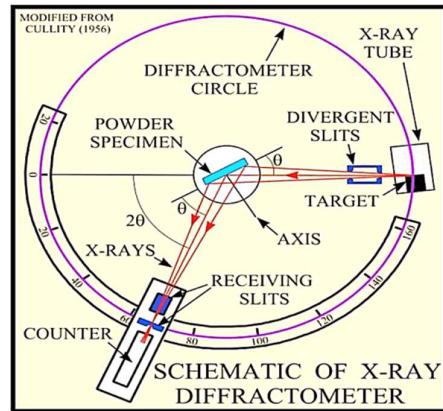


Fig 2.3.2: Schematics of X-ray diffractometer^[10]

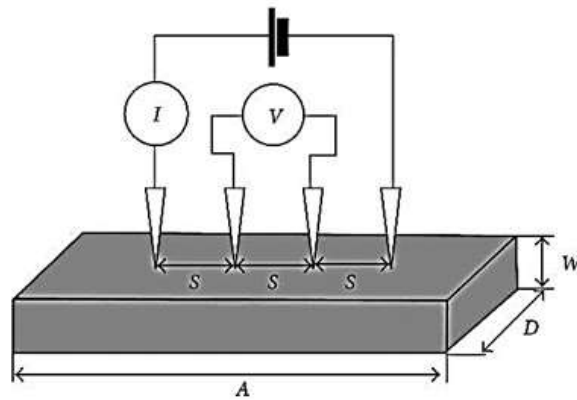
In present study, the powder X-ray diffraction measurements are performed on powder samples using Rigaku X-ray diffractometer.

Powder method is used wherein the annealed sample were grinded manually in a mortar pestle to a sufficiently fine consistency. The powder was packed in to a sample holder (X-ray slides). Although the X ray source produces two wavelengths namely Cu K(α_1), $\lambda=1.54059^\circ\text{A}$ and Cu K(α_2), $\lambda=1.54301^\circ\text{A}$. The average of Cu K(α_1) and Cu K(α_2) were taken that is Cu K(α) $\lambda=1.5418^\circ\text{A}$ was used for determining XRD data on the sample.

The patterns were recorded in continuous mode in the 2θ range of $20^\circ \leq 2\theta \leq 100^\circ$ with a step size of 0.02 at a speed of $2^\circ/\text{min}$ and also the diffraction peaks were indexed using a commercially available Powder Diffraction Package

2.4 FOUR PROBE RESISTIVITY

In the investigation of the electrical properties, four-probe setup was utilised to measure the resistivity of the alloy. The resistivity set up consist of sample holder with four equidistant copper contacts in which, the outer two probes provide for passing current while the inner two are for measuring the induced voltage, constant current generator, power supply and digital screen for measuring voltage and current across the probes.^{[1][3]}



2.4.1 Four probe resistivity setup ^[11]

The rectangular slab of sample was mounted on the sample platform using G-varnish (it electrically isolates the sample from the rest of the sample holder that provides good thermal contact. Four copper contacts are made linearly on the sample surface using fine slurry of silver paint. A manganin heater wound just below the sample holder serves to control the temperature of the sample. A constant current (depending on the resistance of each sample at room temperature) is supplied through Keithley 224 sourcemeter which is connected to two outer probes of the sample, and potential drop is measured by Keithley 2182 nanovoltmeter connected to two inner probes. The measured resistance (V/I) is converted into resistivity.^[7]

The resistivity is calculated using,

$$\rho = R \frac{A}{L}$$

Where, A is the area of cross section and L is the length of the sample.

The entire system is evacuated and cooled to 30K and the temperature is measured with a calibrated Si diode sensor connected to a Lakeshore temperature controller. Using this set-up measurement in the temperature range of 30K to 300K can be made using an in house developed VB program having heating/cooling rate of 5 deg/min.

REFERENCES

- [1] Singh, Sandeep. "Properties of Ni-Mn based Heusler alloys with martensitic transition." (2014).
- [2] http://home.iitk.ac.in/~anandh/lab/Arc_Melting.pdf
- [3] Kargeti, Kuldeep, Ankit Kargeti, and P. K. Mukhopadhyay. "Synthesis of Ni-Fe-Al Heusler alloys and study of their microstructure and FSMA nature." *STUDENT JOURNAL OF PHYSICS*: 181.
- [4] https://en.wikipedia.org/wiki/Energy-dispersive_X-ray_spectroscopy
- [5] [https://www.deshbandhucollege.ac.in/pdf/resources/1585214200_PHY\(H\)-VI-NANO_MATERIAL-1-AJAYPRATAP.pdf](https://www.deshbandhucollege.ac.in/pdf/resources/1585214200_PHY(H)-VI-NANO_MATERIAL-1-AJAYPRATAP.pdf).
- [6] Bunaciu, Andrei A., Elena Gabriela Udriștioiu, and Hassan Y. Aboul-Enein. "X-ray diffraction: instrumentation and applications." *Critical reviews in analytical chemistry* 45.4 (2015): 289-299.
- [7] Singh, Saurabh, and Sudhir K. Pandey. "Fabrication of simple apparatus for resistivity measurement in high-temperature range 300–620 K." *IEEE Transactions on Instrumentation and Measurement* 67.9 (2018): 2169-2176.
- [8] https://upload.wikimedia.org/wikipedia/commons/thumb/9/9f/EDX_scheme.svg/1024px-EDX-scheme.svg.png
- [9] https://wiki.anton-paar.com/fileadmin/wiki/images/X-ray_Diffraction/Schematic-representation-of-the-Bragg-equation.jpg

[10]<https://www.researchgate.net/profile/Ankurjyoti-Bordoloi/publication/327623886/figure/fig3/AS:725729876643841@1550038894899/figure-of-the-X-ray-diffractometer-is-given-below.png>.

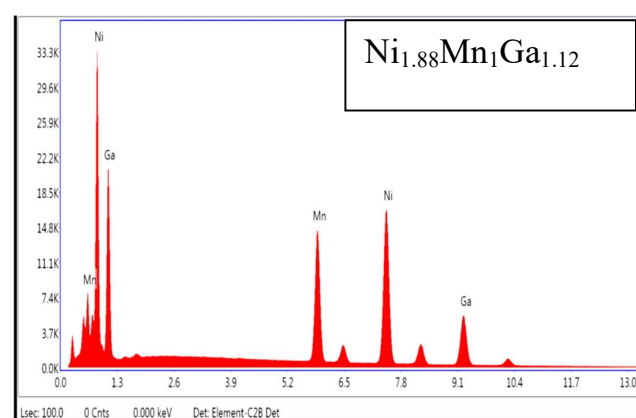
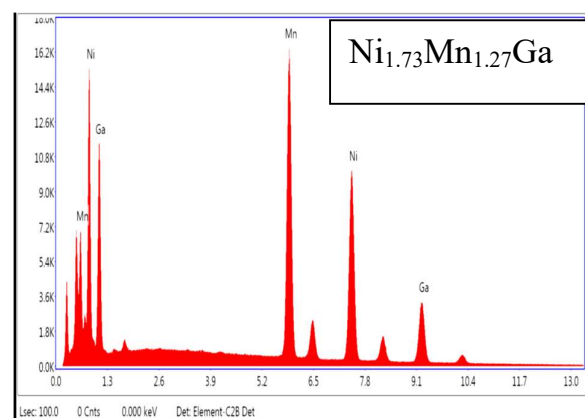
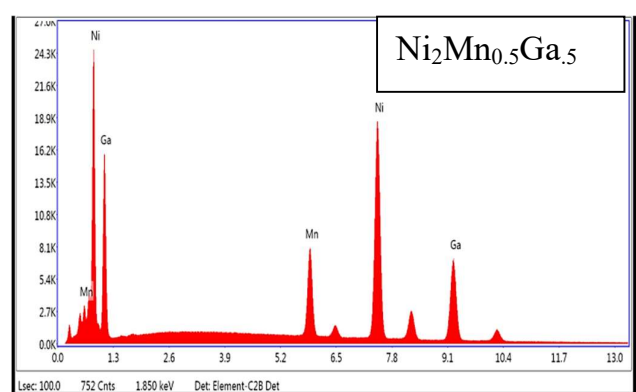
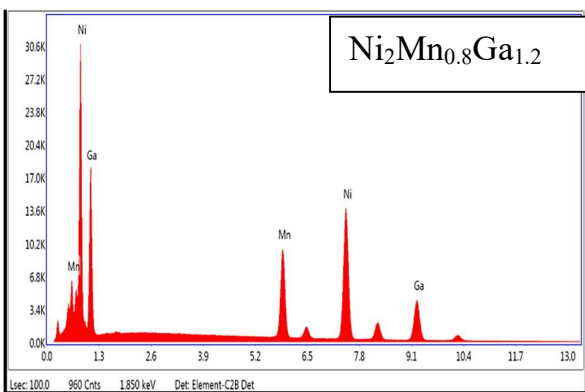
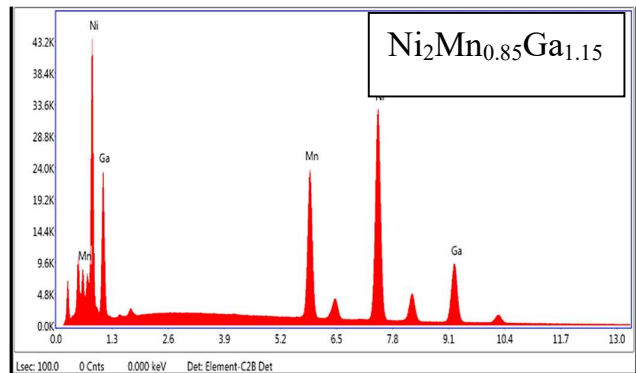
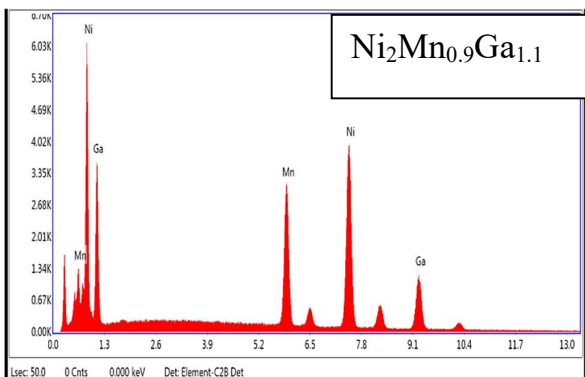
[11] <https://i.imgur.com/9MdvoyX.jpg>

CHAPTER 3

RESULT AND DISCUSSION

3.1 EDAX

To investigate the elemental analysis or chemical characterisation of sample, Energy Dispersive Analysis of X-ray method was performed.



The EDAX data for all six samples are mentioned below,

S.No	Intended Samples	e/a ratio	EDAX Samples	e/a RATIO
1	$\text{Ni}_2\text{Mn}_{0.9}\text{Ga}_{1.1}$	7.4	$\text{Ni}_{2.006}\text{Mn}_{0.91}\text{Ga}_{1.08}$	7.41
2	$\text{Ni}_2\text{Mn}_{0.85}\text{Ga}_{1.15}$	7.35	$\text{Ni}_{2.071}\text{Mn}_{0.852}\text{Ga}_{1.07}$	7.47
3	$\text{Ni}_2\text{Mn}_{0.8}\text{Ga}_{1.2}$	7.3	$\text{Ni}_{2.022}\text{Mn}_{0.81}\text{Ga}_{1.16}$	7.33
4	$\text{Ni}_2\text{Mn}_{0.5}\text{Ga}_{1.5}$	7	$\text{Ni}_{2.06}\text{Mn}_{0.49}\text{Ga}_{1.44}$	7.08
5	$\text{Ni}_{1.73}\text{Mn}_{1.27}\text{Ga}_1$	7.297	$\text{Ni}_{1.562}\text{Mn}_{1.522}\text{Ga}_{0.92}$	7.26
6	$\text{Ni}_{1.88}\text{Mn}_1\text{Ga}_{1.12}$	7.29	$\text{Ni}_{1.90}\text{Mn}_{0.9668}\text{Ga}_{1.1332}$	7.29

Table 3.1.1: Intended and Actual Composition obtained from Energy Dispersive Analysis of X-ray.

The Intended and the Actual compositions obtained from Energy Dispersive Analysis of X-ray (EDAX) for $\text{Ni}_2\text{Mn}_{(1-x)}\text{Ga}_{(1+x)}$ ($x= 0.1, 0.2, 0.5, 0.15$), $\text{Ni}_{(2-x)}\text{Mn}_{(1+x)}\text{Ga}$ ($x=0.27$) and

$\text{Ni}_{(2-x)}\text{MnGa}_{(1+x)}$ ($x=0.12$) are shown in table 3.1.1. The actual compositions obtained are in good agreement with intended compositions. The e/a ratio of the actual composition were found to be approximately equal to intended samples.

$\text{Ni}_{1.562}\text{Mn}_{1.522}\text{Ga}_{0.92}$ composition obtained from EDAX is not in good agreement with the intended composition $\text{Ni}_{1.73}\text{Mn}_{1.27}\text{Ga}$.

3.2 XRD DATA

The room temperature X-ray diffraction pattern (XRD) using $\text{CuK}\alpha$ radiation of

$\text{Ni}_2\text{Mn}_{1-x}\text{Ga}_{1+x}$ ($x=0.1, 0.2, 0.5, 0.15$), $\text{Ni}_{2-x}\text{Mn}_{1+x}\text{Ga}$ ($x=0.27$), $\text{Ni}_{2-x}\text{MnGa}_{1+x}$ ($x=0.12$) is shown in the fig 3.2.1

The Rietveld refinement using jana2006 is performed to find out the crystal structural and lattice parameter.

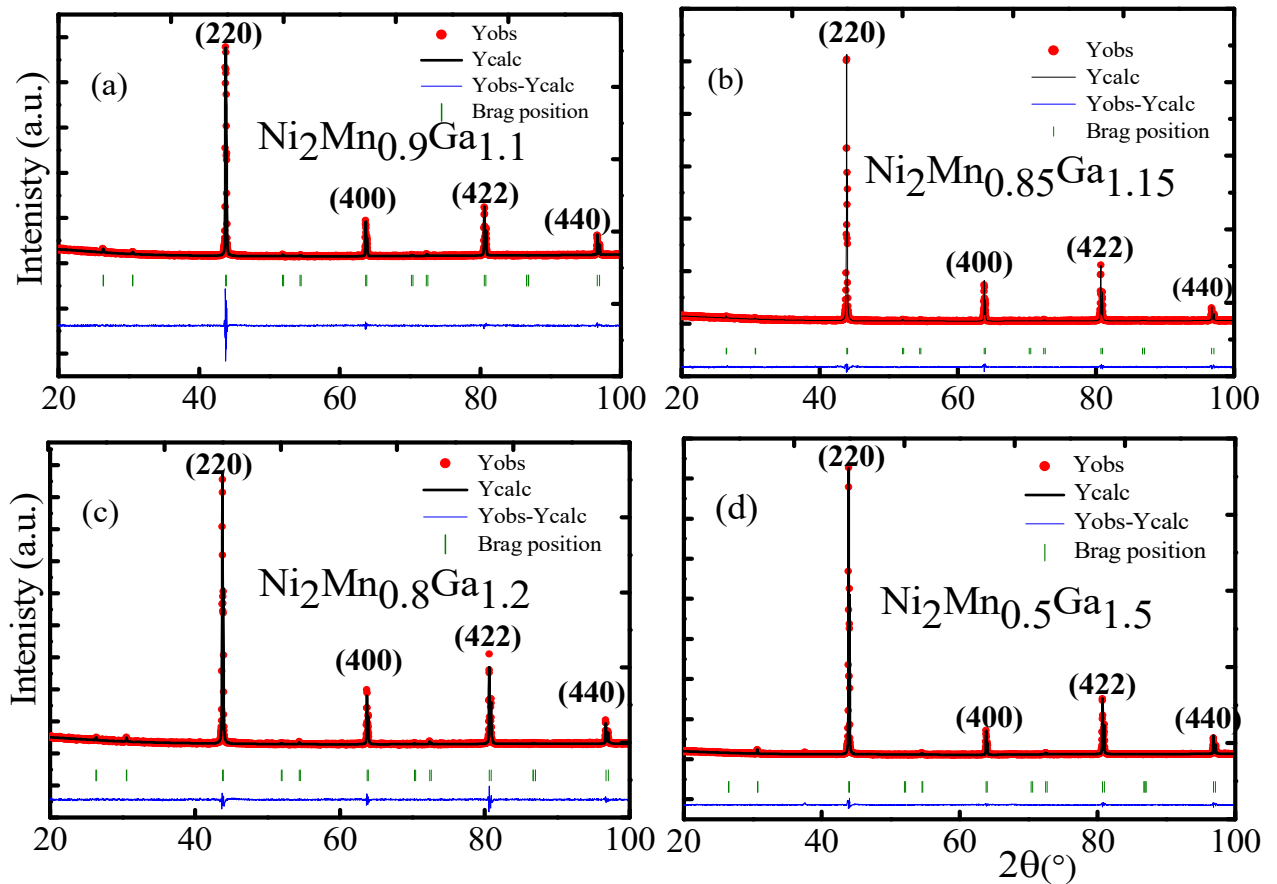
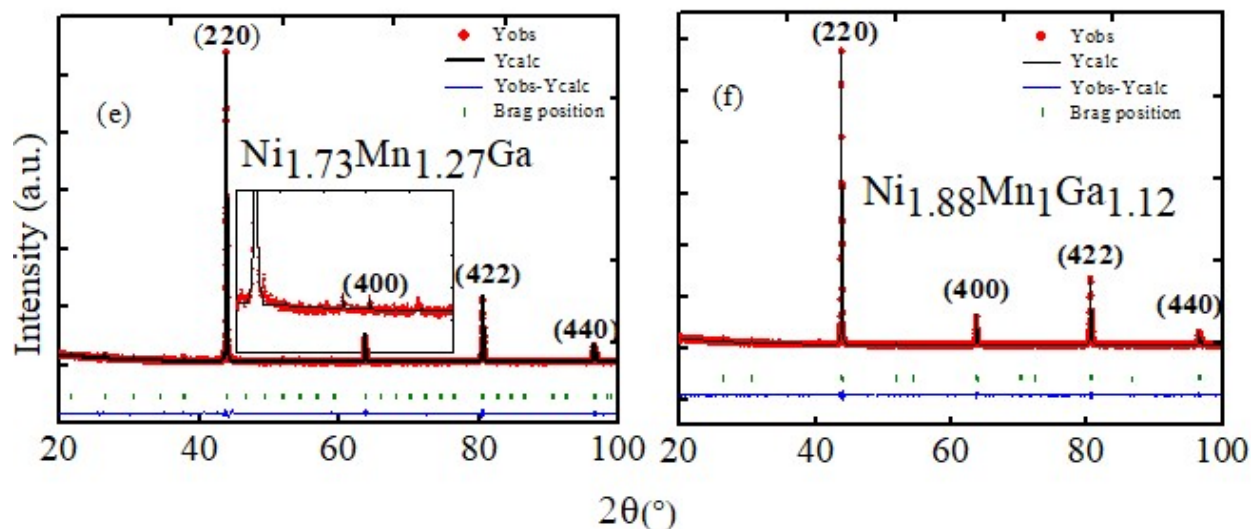


Figure 3.2.1: Room Temperature XRD patterns of samples (a) $\text{Ni}_2\text{Mn}_{0.9}\text{Ga}_{1.1}$, (b) $\text{Ni}_2\text{Mn}_{0.85}\text{Ga}_{1.15}$, (c) $\text{Ni}_2\text{Mn}_{0.8}\text{Ga}_{1.2}$, (d) $\text{Ni}_2\text{Mn}_{0.5}\text{Ga}_{1.5}$



**3.2.1: Room Temperature XRD patterns of samples (e) $\text{Ni}_{1.73}\text{Mn}_{1.27}\text{Ga}_1$,
(f) $\text{Ni}_{1.88}\text{Mn}_1\text{Ga}_{1.12}$**

Fig 3.2.1, shows the XRD pattern for all the samples that exhibits cubic L_{21} structure with $Fm-3m$ space group at room temperature with its regular (220), (400), (422), (440) peaks and lattice parameters given in table 3.2.1. This shows that at room temperature all the samples are in the austenite phase.

For the composition $\text{Ni}_{1.73}\text{Mn}_{1.27}\text{Ga}$ its near to be as $\text{Ni}_{1.5}\text{Mn}_{1.5}\text{Ga}$ so for this we got an extra peaks.

Table3.2.1: lattice constant for all samples

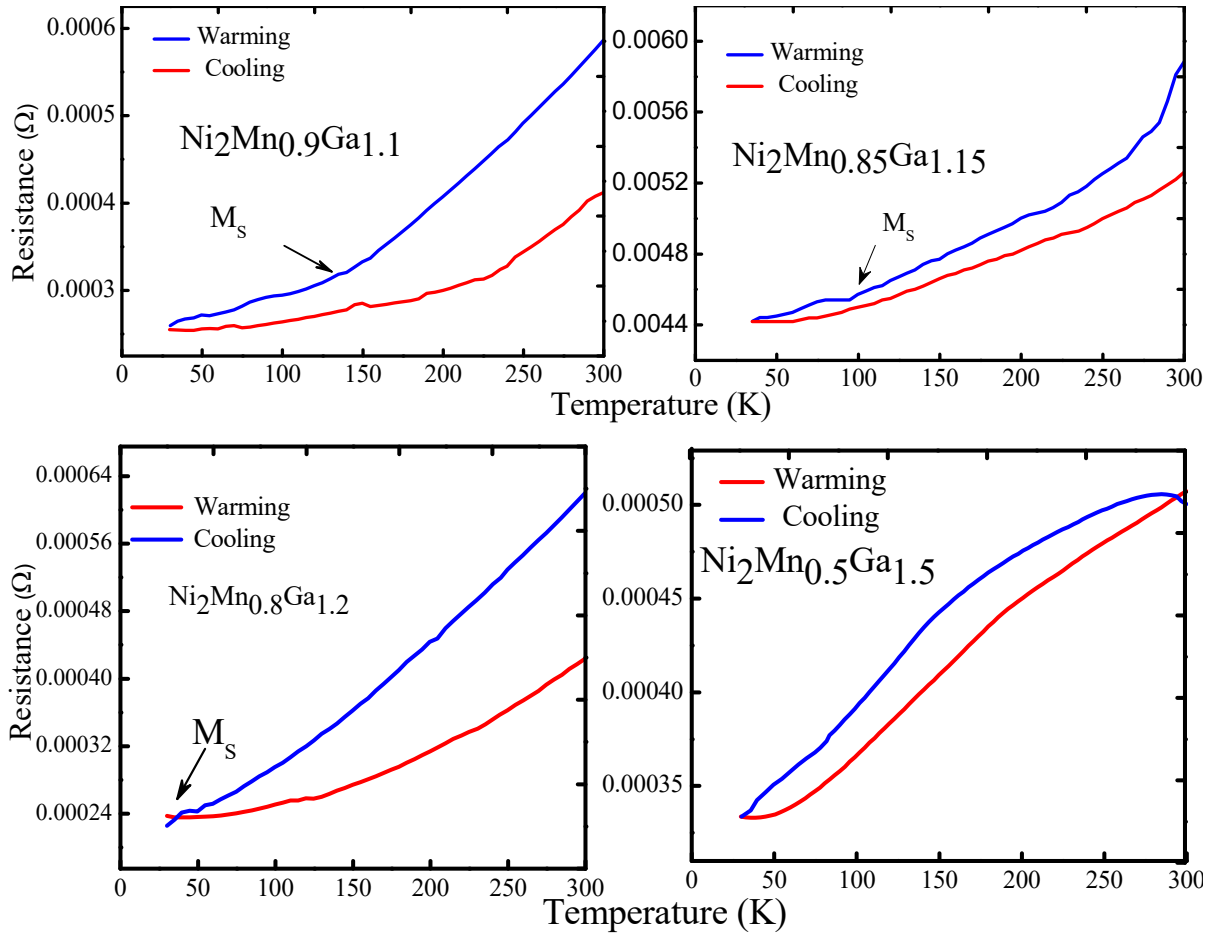
S.NO	Samples	Lattice constant (Å)from Jana	Lattice constant (Å) calculated
1	$\text{Ni}_2\text{Mn}_{0.9}\text{Ga}_{1.1}$	5.827	5.839
2	$\text{Ni}_2\text{Mn}_{0.85}\text{Ga}_{1.15}$	5.829	5.829
3	$\text{Ni}_2\text{Mn}_{0.8}\text{Ga}_{1.2}$	5.822	5.835
4	$\text{Ni}_2\text{Mn}_{0.5}\text{Ga}_{1.5}$	5.825	5.826
5	$\text{Ni}_{1.73}\text{Mn}_{1.27}\text{Ga}$	5.846	5.840
5	$\text{Ni}_{1.88}\text{Mn}\text{Ga}_{1.12}$	5.839	5.838

Table3.2.1: lattice constant calculation for sample1

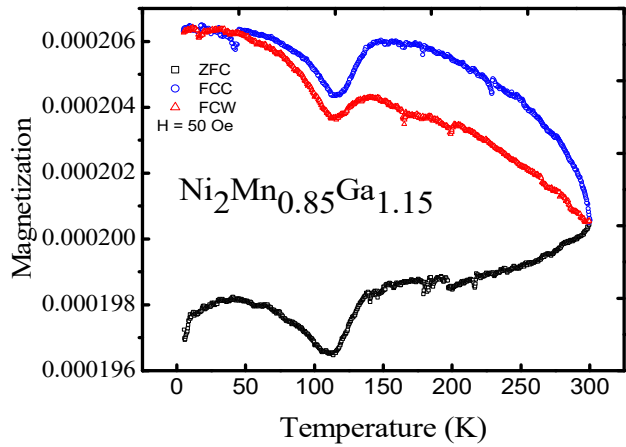
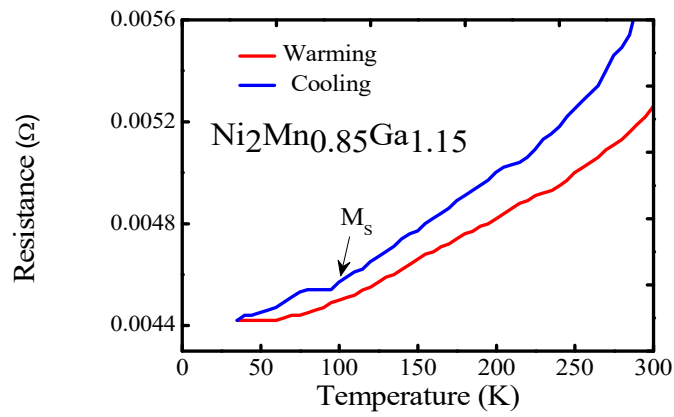
2θ	intensity	θ	Hkl	d(Å)	Lattice constant(Å)
43.74636	23880.34	21.87318	220	2.067623	5.848121
63.68371	4742.218	31.84186	400	1.460073	5.84029
80.56865	6148.195	40.28433	224	1.191343	5.836366
96.63743	3109.057	48.31871	440	1.031391	5.834429

3.3 RESISTIVITY

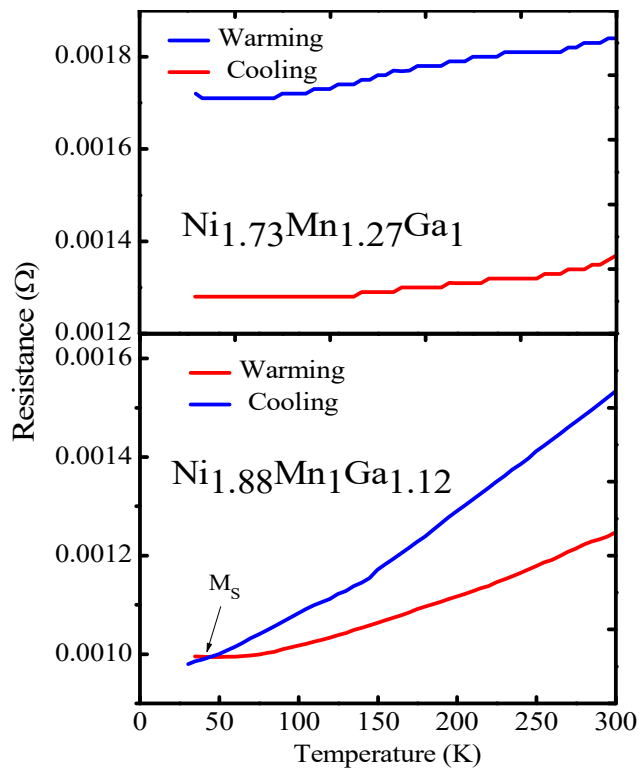
To investigate an estimation of martensitic transformation temperature, resistivity measurement was carried out on all six samples using four-probe resistivity setup.



3.3.1: Resistance plotted as the function of temperature for $\text{Ni}_2\text{Mn}_{0.9}\text{Ga}_{1.1}$, $\text{Ni}_2\text{Mn}_{0.85}\text{Ga}_{1.15}$, $\text{Ni}_2\text{Mn}_{0.8}\text{Ga}_{1.2}$, $\text{Ni}_2\text{Mn}_{0.5}\text{Ga}_{1.5}$



3.3.2 Resistance and magnetisation plotted as the function of temperature for $\text{Ni}_2\text{Mn}_{0.85}\text{Ga}_{1.15}$



3.3.3: Resistance plotted as the function of temperature for $\text{Ni}_{1.73}\text{Mn}_{1.27}\text{Ga}_1$, $\text{Ni}_{1.88}\text{Mn}_1\text{Ga}_{1.12}$

Above figure shows, resistance plotted as a function of temperature, in the range of temperature (30-300 K). For the samples $\text{Ni}_2\text{Mn}_{0.9}\text{Ga}_{1.1}$, $\text{Ni}_2\text{Mn}_{0.85}\text{Ga}_{1.15}$, $\text{Ni}_2\text{Mn}_{0.8}\text{Ga}_{1.2}$, $\text{Ni}_{1.88}\text{Mn}_1\text{Ga}_{1.12}$ and, a narrow hysteresis can be seen. The martensitic start temperature (M_s), by minute hysteresis is nearly equal to 135K, 100K, 50K and 50K respectively, which gives a surety about austenite-martensite transition just below room temperature.

In the sample $\text{Ni}_2\text{Mn}_{0.5}\text{Ga}_{1.5}$ there isn't any indication about the transition in the range of measurements, so that according to the X-ray diffraction the sample remains in the cubic form throughout the whole set of temperatures. The resistivity data confirms that $\text{Ni}_2\text{Mn}_{0.5}\text{Ga}_{1.5}$ is a non-martensitic sample. For the sample $\text{Ni}_{1.73}\text{Mn}_{1.27}\text{Ga}$ there is a compositional variation in the EDAX data when compared with Intended composition. Hence the resistivity data is unpredictable.

CHAPTER 4

4.1 CONCLUSION

We prepared four alloys of the type $\text{Ni}_2\text{Mn}_{1-x}\text{Ga}_{1+x}$ ($x=0.1,0.2,0.5,0.15$) to determine the critical concentration of e/a at which T_M disappears. It shows that $e/a = 7.3$ is the critical concentration. To verify this, we prepared two other alloys $\text{Ni}_{2-x}\text{Mn}_{1+x}\text{Ga}$ ($x=0.27$) and $\text{Ni}_{2-x}\text{MnGa}_{1+x}$ ($x=0.12$) such that e/a ratio is 7.3. From resistivity measurements of the alloys, we confirm that $e/a = 7.3$ is a critical value for Ni-Mn-Ga series

4.1: Critical e/a for Ni-Mn-Z (Z=Sb, Sn, In, Ga)

Z	(e/a)critical	Reference
Sb	8.2	Chapter1(ref.no:20)
Sn	8	Chapter1(ref.no:20)
In	7.85	Chapter1(ref.no:20)
Ga	7.3	Our work

